AD-A244 257

AD-A244 257

DTIC
ELECTE
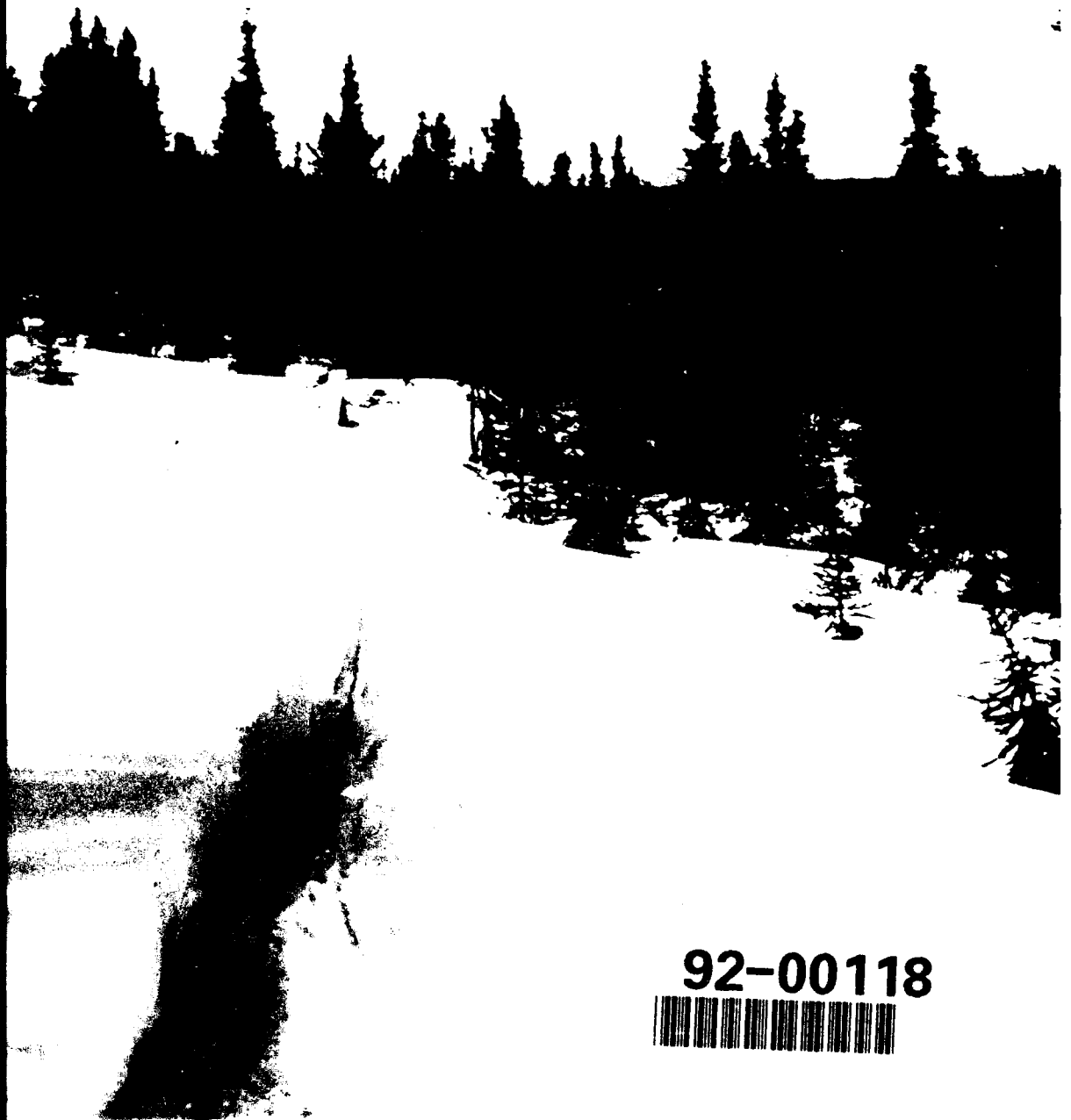JAN 0 3 1992
S D
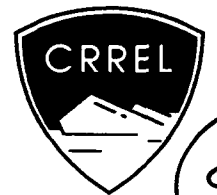
CRREL

Geophysical Investigations of an Anomalous Unfrozen Zone, Caribou Peak, Alaska

Daniel E. Lawson, Steven A. Arcone
and Charles M. Collins

October 1991

92-00118

92 1 2 148

For conversion of SI metric units to U.S./British customary units
of measurement consult ASTM Standard E380, Metric Practice
Guide, published by the American Society for Testing and
Materials, 1916 Race St., Philadelphia, Pa. 19103.

COVER: Radar transect on Caribou Peak.

**U.S. Army Corps
of Engineers**
Cold Regions Research &
Engineering Laboratory

Geophysical Investigations of an Anomalous Unfrozen Zone, Caribou Peak, Alaska

Daniel E. Lawson, Steven A. Arcone and Charles M. Collins

October 1991

PREFACE

CONTENTS

ILLUSTRATIONS

TABLE

Geophysical Investigations of an Anomalous Unfrozen Zone, Caribou Peak, Alaska

DANIEL E. LAWSON, STEVEN A. ARCONE AND CHARLES M. COLLINS

INTRODUCTION

The distribution of permafrost is controlled by a number of interrelated environmental factors and processes. The relationship of these factors and processes in Interior Alaska, where permafrost occurs discontinuously, is complex and poorly defined.

A study was initiated in 1985 by CRREL to examine these relationships in the Caribou–Poker Creeks Research Watershed (Fig. 1), situated in upland terrain north of Fairbanks. Within this watershed, permafrost and non-permafrost terrain can be found having varying slope, aspect, vegetation and elevation, affording the opportunity to analyze the importance of cover and ground conditions in controlling ground temperatures and frozen ground distribution (Collins et al. 1988).

During drilling to install thermistor cable assemblies at representative sites in the watershed, an anomalous unfrozen zone was identified in a borehole located on a north-facing slope. This unfrozen zone was associated with wet conditions that included the flow of a water and sediment mixture or slurry to the ground surface from a depth of about 8.5 m, suggesting a possible relationship to groundwater. Subsequent monthly downhole temperature measurements (described later) also show that these materials remained unfrozen throughout the year.

The presence of unfrozen zones in a north-facing slope is considered an anomaly since the general concept is that north-facing slopes in Interior Alaska are usually continuously frozen while south-facing slopes are free of permafrost.

Geophysical surveys by impulse radar have been used to resolve the groundwater table and special hydrologic features in areas of seasonally and perennially frozen sediments under certain conditions (Annan and Davis 1976, Arcone and Delaney 1987, Arcone et al. 1989, Delaney et al. 1990). Under the hypothesis that the unfrozen zone was caused by groundwater, we undertook an impulse radar survey of the site to determine if the thaw zone could be identified, to define its distribution and to determine its origin. This report presents the results of this survey in light of existing geological and related data, and hypothesizes on the origin of the unfrozen zone.

BACKGROUND

Field site

The Caribou–Poker Creeks Research Watershed is located 48 km north of Fairbanks, Alaska, within the Yukon–Tanana uplands (Fig. 1). This region is characterized by rounded, even-topped hills and ridges with gentle side slopes leading to low relief, alluvium-floored valleys (Wahrhaftig 1965). Bedrock in the watershed consists mainly of quartz–muscovite schist, with lesser amounts of garnet–mica schist and micaceous quartzite of the Fairbanks Schist Unit of the Yukon–Tanana Metamorphic Complex (Forbes and Weber 1982, Robinson et al. 1990). The upper 1 to 20 m of the rock is heavily weathered and covered by colluvium derived from it. Loess thinly mantles the colluvium in some areas, but much of it has been transported downslope and redeposited in valley-bottom fans (Rieger et al. 1972).

Vegetation in the watershed is typical of an Interior, upland boreal forest, with black spruce mainly growing on north-facing slopes and poorly drained valley floors, while aspen, birch, alder and white spruce occupy well-drained soils common on south-facing slopes. Biological communities are locally more complex in response to variations in slope, aspect, drainage and other factors.

Borehole and radar profile locations

Boreholes were drilled in April 1985 at eight locations on the southern and northern faces of Caribou Peak (elev. 773 m) (Collins 1986). Three boreholes are located within the area investigated for this study: K20, K20A and K2 (Fig. 2). Borehole K2 lies at the top of Caribou Peak. Boreholes K20 and K20A lie about 150 m apart along a line trending approximately perpendicular to the slope and located at an elevation of 710 m
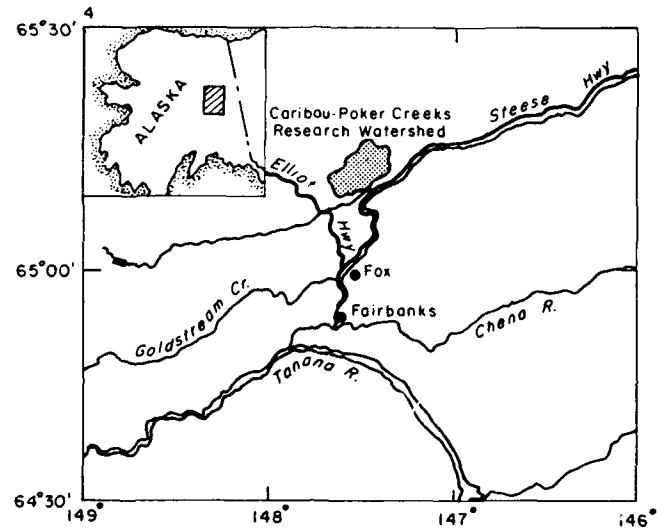
Figure 1. Location map showing the Caribou–Poker Creeks
Research Watershed within the Fairbanks region of Interior
Alaska.
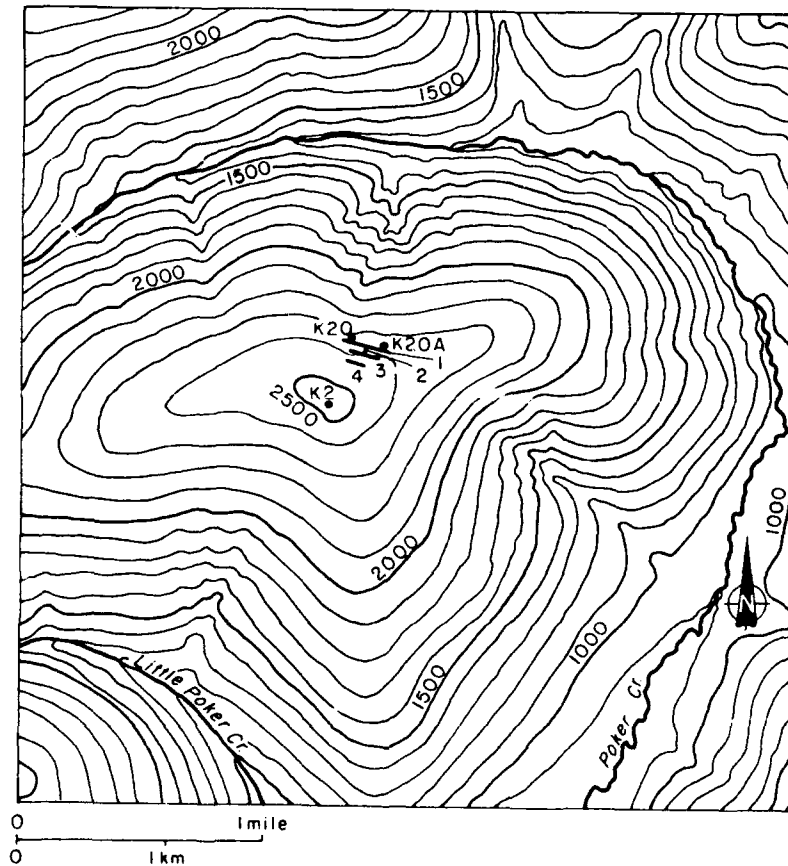
Figure 2. Enlargement of USGS Livengood Quadrangles A-1 and A-2 in the
Caribou Peak vicinity, with the 1985 boreholes located. The approximate
locations of the four transects surveyed by impulse radar are shown. Bore-
holes K20, K20A and K2 lie within the radar surveyed site.

2

about 60 m (400 m distance) below K2 (Fig. 2). The estimated angle of slope increases from 2° near K2 to 10° at K20–K20A and to 15° approximately 30 m below K20–K20A. Borehole K20 occurs within the unfrozen zone, while K2 and K20A penetrate into permanently frozen ground below the active layer. Details of the borehole logs, site vegetation and thermistor installation are presented in Collins (1986) and Collins et al. (1988).

Four transects for impulse radar profiling were established by tape and compass, with the lowermost transect (1) located along a west–east line between K20 and K20A that is perpendicular to the slope (Fig. 2). Transects were radar profiled on 4 April 1990, when snow ranged in depth from 1.5 to 2.5 m (Fig. 3). Snow along each transect was packed down using snowshoes prior to ground profiling. Each transect was profiled twice with two different antenna systems.

Radar instrumentation

General operation

Commercially available short-pulse radar (also known as impulse, subsurface or ground-penetrating radar) consists of a control unit, antennas and cables, a magnetic tape recorder and a power supply. The control unit generates timing signals to key the transmitter on and off and synchronizes this keying with the receiver. It controls the scan rate (how fast individual echo scans are compiled), the time range over which one wants to view the echoes, and the gain to be applied to the echoes. The transmit antenna is excited by a semiconductor device and is designed to radiate a broadband pulse of only nanoseconds duration. Consequently, the antenna produces a low gain radiation pattern. A separate but identical receive antenna is employed because echoes can return from near-surface targets before the transmit antenna has stopped radiating. Electronics for the transmitter and receiver are usually incorporated into the antenna housing. The VHF–UHF received signals are converted by sampling into an audio frequency facsimile for filtering, amplification and recording. Data can be simultaneously displayed or quickly played back in strip chart form. Digital recording was used in this study, along with packaged signal processing software that permits several filtering functions and data display formats.

Control unit

The radar system used was manufactured by the GSSI company (Geophysical Survey Systems, Inc., North Salem, New Hampshire). The control unit was a

Figure 3. A part of transect 3. The snow on each transect was trampled with snowshoes before radar profiling. Vegetation is typical of the northern face of Caribou Peak.

3

SIR Model 4800 mainframe that triggers pulses at a repetition frequency of approximately 50 kHz and compiles the received pulses into 25.6 scans/second (higher or lower rates are possible). A variety of range gain functions may be applied over the time duration of the scans to suppress the higher amplitude, early returns (especially the direct coupling between transmit and receive antennas) and enhance the lower amplitude, later returns. The control unit also controls the time range of the scans, which can be varied from tens to thousands of nanoseconds. An event marker is available to mark distance on the radar record.

Antennas

Two antenna sets (Models 3102 and 3105, GSSI, Inc.) operating over different frequency bands were used in this study.

A typical radiated wavelet (Fig. 4) for both antenna units is commonly characterized by the frequency corresponding to the period of one oscillation: 500 MHz for the 3102 radiating in air and about 300 MHz for the 3105, with both waveforms having a bandwidth of about 50%. When directly coupled to the packed snow, these frequencies lowered to about 330 and 150 MHz respectively. Our use of two different frequency bands was motivated by our interest in achieving high resolu-

tion near the surface with the 3102, and deeper penetration with the 3105, the lower frequency of which would experience less attenuation from scattering and conductive absorption.

Both transmit and receive antennas were housed in single units, in which they are adjacent and backshielded. The antennas are flared dipoles with a resistive loading to inhibit current oscillation, and are excited by a transmitter that radiates about 8 W (3102) and 5 W (3105) peak power as rated by the manufacturer. Subsurface radiation patterns for either antenna design are believed to be multilobed based on the theoretical results for point dipoles by Engheta et al. (1982). This theory shows a strong lobe of energy to be confined within the angle $\psi = 2\sin^{-1}(1/n)$ measured about vertical, where n is the real part of the refractive index of the ground. For frozen ground of high ice content, n might typically be 2.3 so that $\psi = 52°$.

Data processing, display and interpretation

All data were recorded in scans of 512 eight-bit words on a GSSI DT6000 tape recorder. The recorder can be read onto a personal computer by a software program (Boucher and Galinovsky 1989) that also processes the data. The program is capable of a variety of filter functions, both horizontal (i.e., over distance or
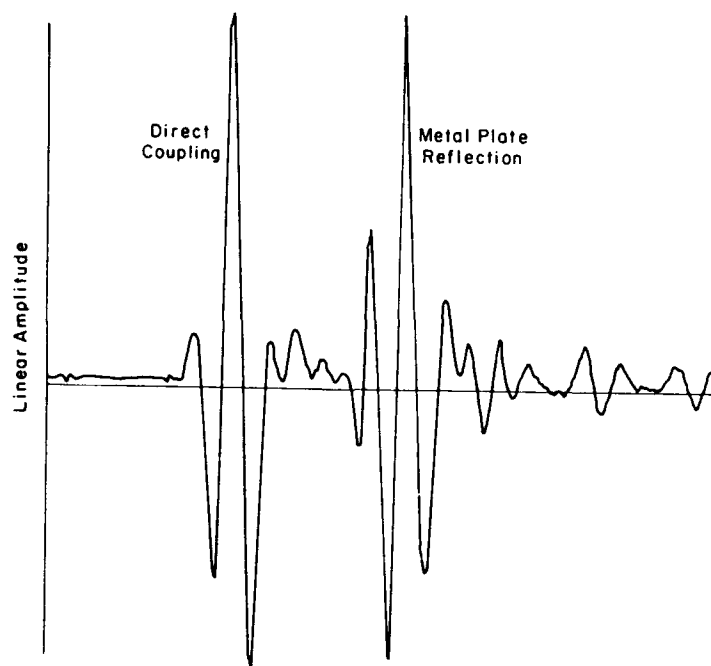

Figure 4. Typical waveform of the radar pulse emitted from either the Model 3105 or 3102 antenna units. The time scale is arbitrary.
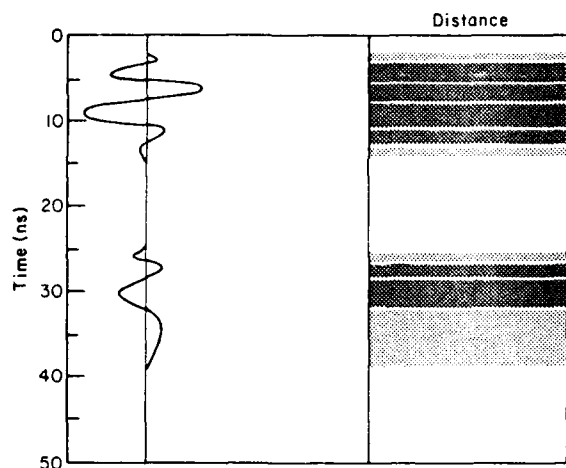
4

Figure 5. Wiggle trace display (left) of a single scan and equivalent graphic record (right) should these scans remain constant with profile distance.

equivalently, many scans) and vertical (i.e., over time, or equivalently, along one scan). Data can be displayed in either a wiggle trace (amplitude versus time of each scan) or line scan (intensity as color or darkness versus time) format as shown in Figure 5. Individual scans are easily retrievable with the software. Interpretation of data is generally based on the simple echo delay formula

$$d = ct/2n \qquad (1)$$

where d is the depth of a reflector in centimeters, t is the echo time delay in nanoseconds and c is the speed of electromagnetic waves in a vacuum (30 cm/ns). The quantity n is often replaced by $\sqrt{\varepsilon}$ where ε is the dielectric constant. The factor of two in eq 1 accounts for the round trip propagation path of the pulse. Equation 1 applies only to reflections emanating from horizontally flat interfaces of several in-situ wavelengths extent, or to scattering from point sources. It can be applied to several layers successively if n is known for each layer and the time delays to each layer interface are easily picked off the record.

The dielectric constant of frozen or unfrozen earth materials as a function of water content in the 100- to 1000-MHz range has not been extensively investigated in comparison to the wide variety of material types that exist. Generally, competent crystalline rocks can range from $\varepsilon = 4$ (quartzite) to 6 (felsic granites) to 9 (marble or basalts; e.g., Campbell and Ulrichs 1969) with little dependence on water content as it is generally less than 1% of the volume of the material. There are no data available for deeply weathered bedrock, but it should be

similar to the properties of soil for which there are extensive data, both laboratory and field. These investigations have shown that ε of unfrozen wet soils (sands, silts, clays, loams) will monotonically increase with increasing water content, and will range from about 2.6 when dry, to about 36 at saturation (e.g., Topp et al. 1980), with dielectric loss increasing in similar proportion. In contrast, the ε of frozen soils will increase only until about 40% water content is reached, beyond which ice begins to replace unfrozen adsorbed water (which is significant in silts and clays) and thus decreases ε (e.g., Arcone and Delaney 1989, Delaney and Arcone 1984). Typically, ε for the high ice content sands, silts and gravels of Interior Alaska ranges between 4 and 6. Massive ice, of course, has an $\varepsilon = 3.2-3.5$ and a dry snowpack about 1.2–1.4 (Cumming 1952) for typical densities of a seasonal ground cover.

Reflections that strongly slope or curve with the horizontal profiling distance must be "migrated," a complicated process of diffraction summation that derives the correct orientation of reflectors from the radar time–distance data. Migration is a straightforward procedure when there is only one layer of interest. For a more complicated layer structure in which n may vary continuously within the space of a few in-situ wavelengths, exact migration is practically hopeless. Therefore, migration of sloping reflectors in this study will assume a simplified structure for n based upon data available in the above cited references.

Borehole geology

The stratigraphic log of borehole K20 is typical of the watershed uplands (Fig. 6). A 0.15- to 0.18-m organic mat overlies a relatively thick (3.0 m) layer of gravelly colluvium containing very angular rock fragments, which in turn overlies a 0.4-m layer of gravelly silt. This horizon overlies quartz–muscovite schist bedrock, which is weathered to a depth of about 13.9 m (Collins 1986). Moderately weathered bedrock grades progressively below a depth of about 10 m to unweathered bedrock at 13.9 m where auger refusal occurred. It should be noted that because of equipment limitations, the drill was unable to penetrate into sound bedrock. This limitation, however, clearly defines the depth of weathering at each site.

The ground was frozen to 3.0 m depth, where an unfrozen layer of gravelly silt was encountered. This localized layer remained unfrozen until May 1989, when measurements indicated that ground temperatures had gradually decreased over several months to below 0°C. The gravelly silt horizon was therefore classified as frozen during this radar study, but not so strongly as to seriously depress the dielectric constant of the material, as will be discussed later. From 3.4 to about 6.0 m, the

5
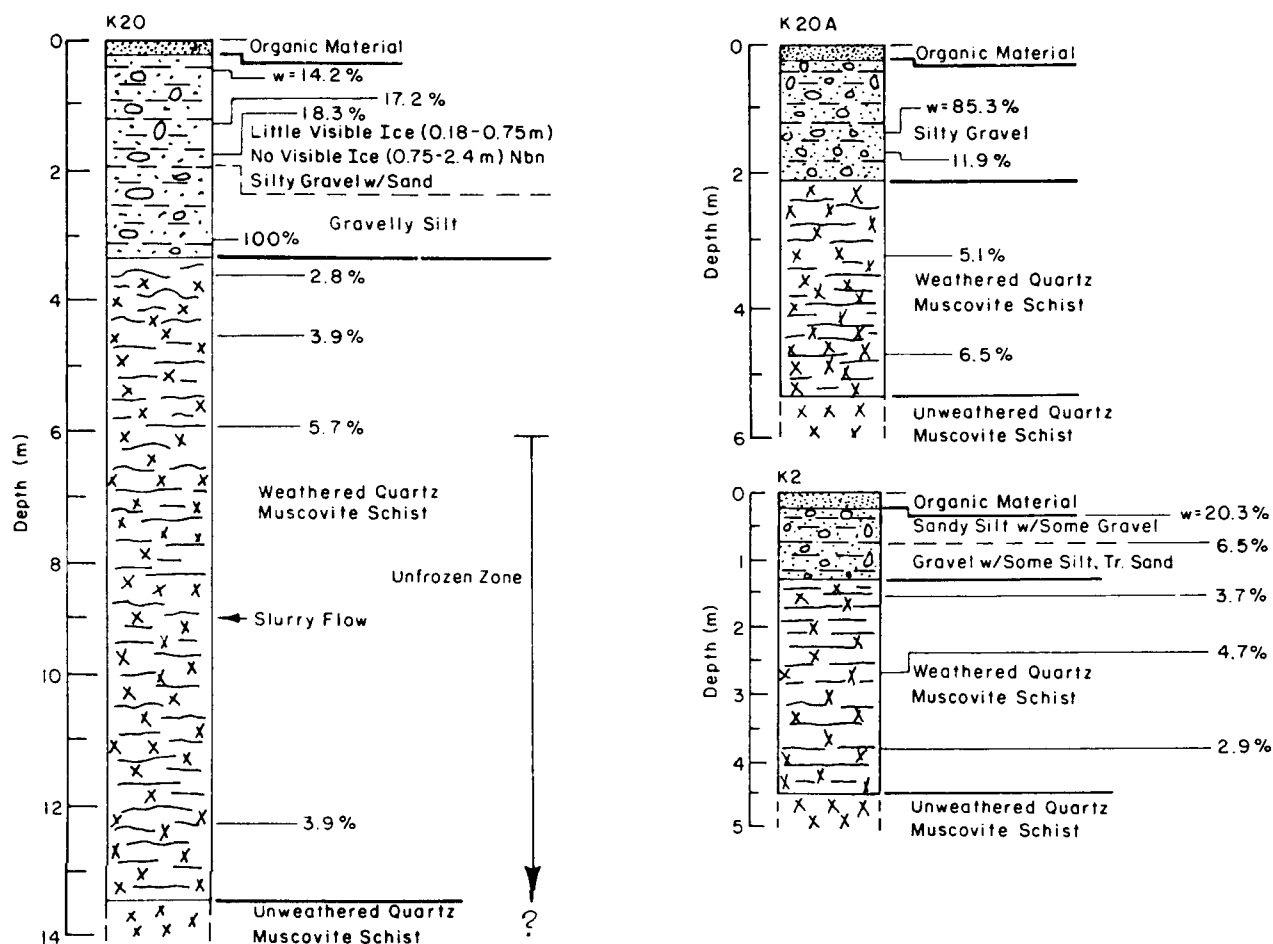
Figure 6. Summary of geologic logs for boreholes K20, K20A and K-2.

weathered bedrock was dry and frozen. Cuttings from depths of 6.0 to 8.5 m appeared moist, but it was uncertain if the bedrock was frozen or unfrozen. Subsequent temperature measurements suggest that the bedrock at these depths is frozen at 6.0 m, but warming to slightly above 0°C by the 8.5-m depth. Extremely wet, unfrozen conditions occurred below 8.5 m. Water containing cuttings and weathered materials flowed to the ground surface as a slurry from a depth of about 8.5 to 9.0 m during the drilling. After 12 hours, water associated with this zone had risen to 5 m depth in the borehole.

Boreholes K20A and K2 were frozen through their approximately 5-m lengths in 1985 (Collins 1986). Unweathered quartz–muscovite schist occurred at a shallower depth in K20A (5.3 m) than in K20, and the overlying colluvium appeared to grade into weathered bedrock from about 2.1 to about 3.5 m (Fig. 6). Borehole K2 consisted of a much thinner (~1.5 m) frozen colluvial layer overlying slightly weathered quartz–muscovite schist; auger refusal occurred at a depth of 4.6 m.

RESULTS AND DISCUSSION

Radar profiles

Seven radar profiles ar presented in wiggle trace format, three for the 330-MHz 3102 antenna unit and four for the 150-MHz 3105 unit. The extra 3105 profile was run perpendicular to transects 1 and 3. On each profile, the horizontal direction is distance along the transects and the vertical direction is echo time of return. Each profile was processed with a horizontal high-pass, "background removal" filter to eliminate noise bands, and a vertical high-pass filter to eliminate variations in overall signal level from scan to scan caused by changes in coupling between antenna and snow surface because of uneven towing of the antenna. All profiles were also horizontally justified in that the number of scans between distance marks was equalized.

The events on the records are classified either as horizons, which are generally horizontal and extend across the entire record, or as dipping reflectors that

6

might either be real, or apparent, as would be caused by air or snow refractions. The horizons are composed of intermittent reflections that occur frequently enough to indicate a vertical transition in material properties, whereas the reflections from the dipping structures are much stronger and more consistent. The 150-MHz profiles have longer time scales (as allowed by the data digitization rate) to look for deeper reflections. Therefore, similar events in both profiles only appear to occur at different depths or have different time–distance slopes.

Figure 7 shows the 150- and 330-MHz profiles along the 190-m transect 1, which passed directly adjacent to boreholes K20 and K20A (Fig. 2). The 330-MHz record has a shorter time duration and therefore the events are better separated than in the 150-MHz record. The first horizon (number 1) is the direct coupling between the transmit and receive antennas and serves as a 0-ns reference for timing the later events. Horizon 2 is the base of the snow cover and generally occurs at about 5- to 7-ns delay. If the trampled, seasoned snowpack has a density of about 0.35, the corresponding dielectric constant is about 1.4 (Cumming 1952), which translates the time delays to snow depths of 89–124 cm.

Horizon 3 is far less consistent and appears mainly as a darkening of the record; it is more obvious in the 330-MHz profiles of transects 2 and 3 shown later. We interpret this horizon as a transition within the colluvium and not between the colluvium and weathered bedrock, which is far too deep (3.0–3.4 m) to give a meaningful dielectric constant for the time delay of about 25 ns near K20. Using a dielectric constant of about 4.8, as measured in gravelly alluvium (Arcone and Delaney 1989) of similar water content (5–30% by weight) and temperature (0 to –1°C), places this horizon at a depth of about 1.7 m below the ground surface. Therefore, this horizon more likely indicates a seasonally derived transition from low (about 3% or less) to high (about 3–6%) volumetric unfrozen water content, as is known to occur in fine-grained sediments (Hoekstra et al. 1975); a few percent change in unfrozen water content has been shown both theoretically and experimentally by Delaney and Arcone (1984) to approximately double the dielectric constant. This horizon is deeper further across the record, reaching a depth of about 2.1 m near K20A. The transition in unfrozen water content cannot be deduced from the drill log that documents only total water content in cuttings at specific locations. There is no distinct horizon for the colluvium-to-weathered-bedrock transition, which suggests that the weathered bedrock has a dielectric constant similar to that of the marginally frozen, lower layer of colluvium.

The most conspicuous features in both the profiles of Figure 7 are the dipping reflectors. Those that dip most steeply either to the east or west (e.g., event 4) are

refracted air waves traveling along the air/snow boundary and reflected back to the antenna. This source is deduced from the time/distance slope, which gives a one-way wave velocity very close to 30 cm/ns, the speed of radio waves in a vacuum. The stronger reflections (e.g., events 5 and 6), which all dip to the east, are believed to be legitimate linear features that are probably water within fractures in the bedrock, which drill logs suggest is moderately to slightly weathered. Three primary planes appear evenly spaced at about 55 to 60 m. The steepest planar feature at 0 to 8 m along profile 1 is a multiple of the feature to its right. In either profile, the strongest part of these events occurs at a time delay of about 120 ns between stations 20 and 30 m (event 6). At this point there is also the peak of a hyperbola, which indicates a strong, localized concentration of water, as might occur in an open fracture.

Since fractures would be characteristic of only the bedrock, we may assume that the start of these features indicates the colluvium/weathered bedrock interface. These features seem to originate at progressively greater depths from the surface when moving from west to east across Figure 7, but the exact depths cannot be determined since we have no independent measure of the dielectric constant of the entire column of colluvium. Nor is the dielectric constant of the weathered bedrock known, which is needed to determine the dip angle of the fractures. However, this latter constant need only be roughly estimated to find an approximate dip angle.

In a homogeneous medium, the apparent dip angle α in nanoseconds per meter measured from horizontal in a time–distance plot is related to the true dip angle β in a depth–distance plot through the migration relationship

$$\beta = \sin^{-1}(c\tan\alpha/2n). \tag{2}$$

This angle will not change on the radar record if there is an overburden of constant depth and dielectric profile situated above the medium containing the fracture. If there were a direct correspondence in scale of 1 m = 1 ns, the apparent fracture angle α in Figure 7 would be approximately 64°. As there is no evidence of a strong bedrock–colluvium reflection, and the reflection within the colluvium is weak at best, n for the weathered bedrock probably varies only between about 2 and 3, confining β to between 6 and 9°.

Borehole K20 encountered water at a depth of about 8.5 to 9.0 m. Using $n = 2$ for the weathered bedrock, which gives a true dip angle $\beta = 9°$, would place the radar planar feature at about 8–9 m below the ground surface at K20 and, thereby, links the wet, unfrozen zone directly to these dipping reflectors. The similarity in
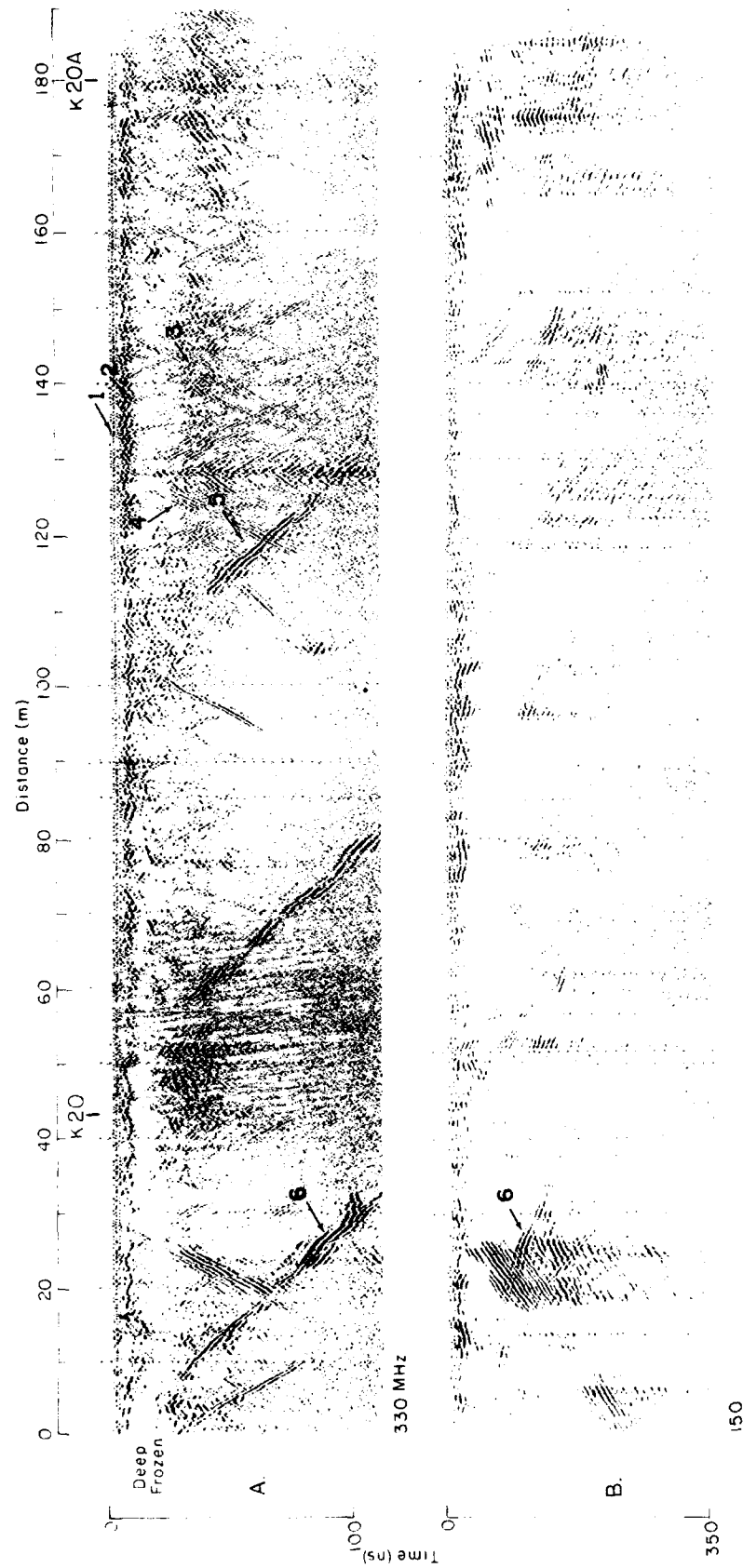
7

Figure 7. Processed radar profiles of transect 1. Boreholes K20 and K20A are located. Processing and explanations of the numbered events are described in the text. The strong, relatively planar signatures dipping to the right (east) are interpreted as water-filled fractures within the bedrock. a. 330-MHz 3102 antenna. b. 150-MHz 3105 antenna.

8
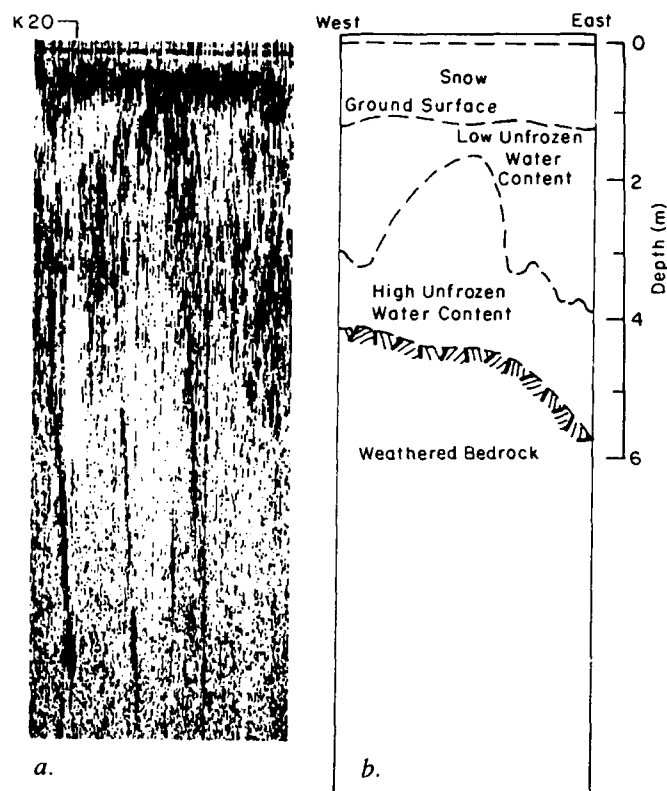
Figure 8. 330-MHz profile of transect 1, with additional stacking and filtering (left), to better illustrate features of interest as interpreted on the right.

returns of the other planes indicates that they are also probably filled with water at depth. Downhole temperature data provide further evidence on the nature of this zone and are discussed later.

Figure 8a is a highly processed version of Figure 7a, and its interpretation, which summarizes many of the ideas presented above, is given in Figure 8b. The data of Figure 8a were first stacked six-fold and then processed using a Hilbert magnitude transform, which is, basically, an energy envelope detection scheme. The purpose of the stacking is to compress the data horizontally to bring out the horizons. Figure 8b interprets the horizons of Figure 8a as the base of the snow layer, a transition from low to high unfrozen water content within the colluvium (horizon 3, Fig. 7a), and the weathered bedrock as interpreted from the start of the fracture events. The low-to-high unfrozen water transition is seen to rise in the middle of the record and deepen towards the east. This rise in the center of the record implies that borehole K20 is not located where the warmest zone comes closest to the surface along this profile.

Two additional transects (transects 3, 4; Fig. 2) were profiled to determine if the planar features at transect 1 were highly localized or more continuous. Each of the two profiles that lie parallel to transect 1 exhibit several planar features, with the strongest continuous reflection correlating precisely with the structure intercepted by borehole K20 (Fig. 9). Profile 3, located 60 m upslope of profile 1, also has a strong return at depth (about 110–130 ns) that appears to correlate with the middle signature (60–80 m) on profile 1. The planar signature furthest east on profile 1 (about 122 m) is not as strong a reflection and also does not appear to have been encountered on transect 3. This absence may simply have resulted from transect 3 being of insufficient length to have passed over it. Similarly, on transect 4, the profile reveals a single, strong planar reflector that we have correlated with the middle signature on profile 1. The partial feature on the north end of transect 2, which is perpendicular to transect 1, may correlate with a fourth, only partial return at approximately 105 m distance and 110 ns depth on line 1, but this is not certain; no correlative signature occurs on either profiles 3 or 4.

9
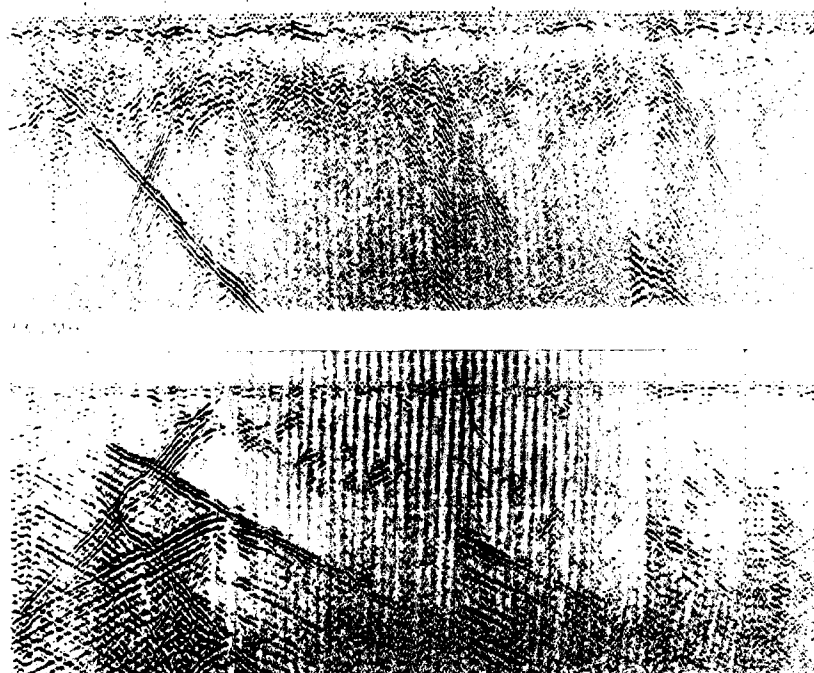
a. Comparison between 3102 and 3105 returns for transect 3.

Figure 9. Processed radar profiles of transects 2, 3 and 4. Locations are shown on Figure 2.
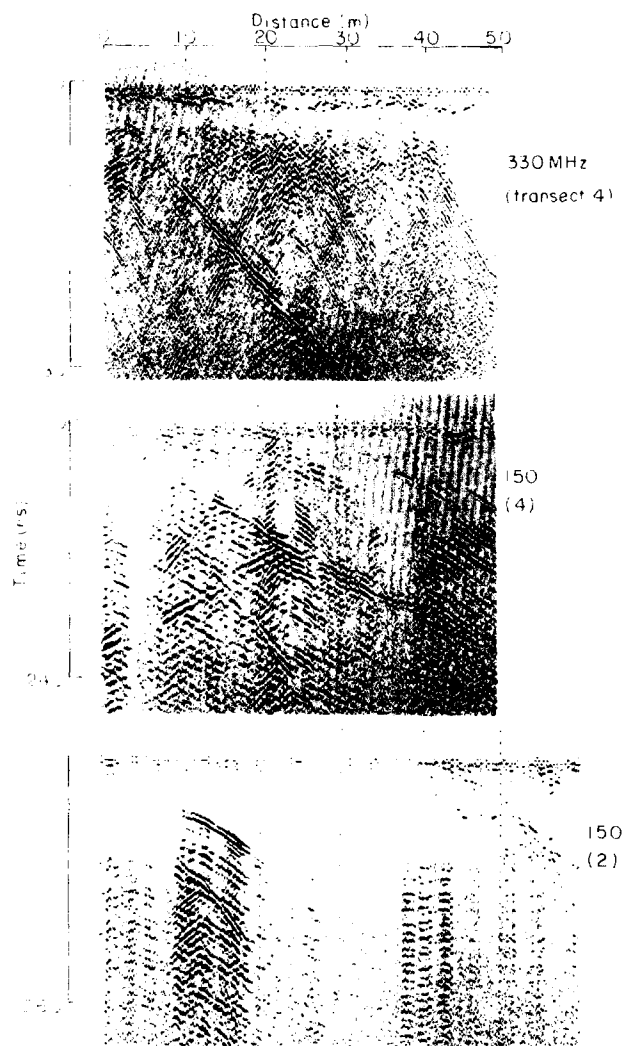
b. Comparison between 3102 and 3105 returns for transect
4 and the 3105 returns for transect 2.

Figure 9 (cont'd).

11
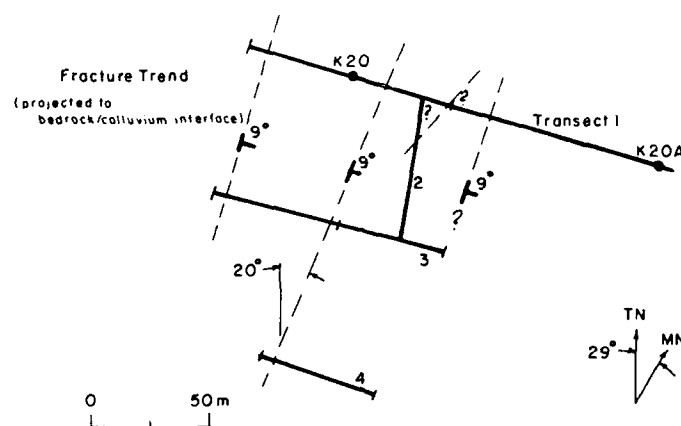
Figure 10. Spatial distribution of fractures relative to radar transects and boreholes. Fractures trend generally N20°E with an easterly dip of about 9°.

The spatial continuity and form of the dipping reflectors are evidence of these features being fractures, or possibly joints, owing to their relatively consistent spacing, within the bedrock. Forbes and Weber (1982) indicate that bedrock in the crest area forms the east–west trending axis of an overturned or recumbant fold. The fractures apparently occur on its northern overturned limb and may be associated with this deformation.

The distribution of the fractures and their apparent correlation from profile to profile at a given depth (in ns) indicate that they trend roughly N20°E, upslope and downslope, at this site. The apparent convergence of the two best defined fractures may be real or be ascribable to ground and bedrock surface relief for which the trends are not corrected (Fig. 10). It is also possible that fractures within the bedrock of the surveyed area are more numerous than displayed by the radar. This possibility is suggested by the apparent lack of continuity of certain signatures from profile to profile. Unless a change in the dielectric constant of the materials results from the presence of water in the fractures, the fractures would probably be indistinguishable from the surrounding weathered bedrock.

The continuity of the fractures upslope and downslope

suggests that groundwater is flowing from a source that is higher in elevation than the area surveyed in this study, or alternatively, may have an aquifer source at depth in the bedrock. Aerial photographs of Caribou Peak during summer (see Fig. 12 later) show both outcrop and vegetation patterns with an approximately parallel north–south trend, suggesting that a relationship exists between drainage from the fractures and the vegetation pattern; this relationship will be considered later.

Groundwater in unfrozen schistose bedrock elsewhere in this region commonly occurs within structural features. Cederstrom (1963) and Péwé and Bell (1975), for example, concluded that its occurrence in the Fairbanks area uplands was commonly controlled by fractures, joints and fractured quartz veins, in some cases being perched above permafrost. Water-bearing structures of this type are generally random in location and frequency of occurrence, and therefore difficult to predict. The radar method now provides one technique for better defining this random distribution.

Downhole temperatures

Ground temperatures have been measured continuously in each borehole since 1986 (Collins et al. 1988).

12

For these measurements the resistances of individually calibrated, precision thermistors are read directly and converted to temperature using the modified Steinhart equation. Measurements are accurate to ±0.05°C, with a system uncertainty estimated at ±0.03°C and a precision of ±0.01°C. Data from K20A, K20 and K2 for the period of January 1987 through December 1989 are summarized in Table 1. Summary graphs of the downhole temperatures for 1989 are shown in Figure 11.

Although the ground temperature data are limited in depth and quantity, qualitative assessments of their bearing on the origin of the unfrozen zone can be made. Three aspects of the temperature data from K20 appear anomalous when compared with the data from nearby boreholes K20A and K2 as well as from other boreholes in the watershed presented in Collins et al. (1988).

The three anomalous aspects of the temperature data are the range and magnitude, the gradient, and seasonal variations. The data suggest that an influx of heat not correlated with seasonal surface warmings or with the geothermal heat flux is affecting the ground temperatures at K20.

Seasonal variations in ground temperatures are highly attenuated within K20. Normally, seasonal variations in air and surface temperatures cause subsurface fluctuations in temperature to a depth of 20 m, where changes are about 0.01°C with a time lag of 1 year (e.g., Gold and Lachenbruch 1973). More rapid responses of larger magnitude occur within the upper 10 m.

Commonly, even though there may be small temperature variations to 20 m depth, the depth of zero annual amplitude Z_z can be assumed to be at about 10 m, where the annual variation is less than 0.1°C, which is less than 1% of the surface temperature annual amplitude (Lunardini 1981). The ground temperature T_z at depth Z_z will generally be less than the mean annual ground surface temperature T_s. Thermal disturbances will modify this relationship (Brown and Péwé 1973). At the crest of Caribou Peak, climatic data indicate that the Mean Annual Air Temperature (MAAT) is about −2.9°C with a Mean Annual Ground Temperature (MAGT) of −1.0°C (Haugen et al. 1982, Collins et al. 1988). At K20A, the mean annual ground temperature is estimated at −1.3°C (Collins et al. 1988). Borehole data suggest the temperature at 10 m depth is about −1.1°C. The MAAT for the K20A site may be estimated using the empirical relationship between MAAT and MAGT of Haugen et al. (1983)

$$MAGT = 0.7\ MAAT + 1.25 \qquad (3)$$

where MAGT is approximately the same as T_z, based upon a number of borehole measurements throughout Interior Alaska. Using a T_z of −1.1°C for MAGT, we estimate the MAAT value to be −3.6°C.

Given the proximity of holes K20A and K20, and the sites' general similarity in elevation, aspect, slope angle and vegetation, the MAAT and ground temperatures and their variations should be similar in both holes. Measurements in hole K20, however, indicate relatively high ground temperatures and seasonal variations that
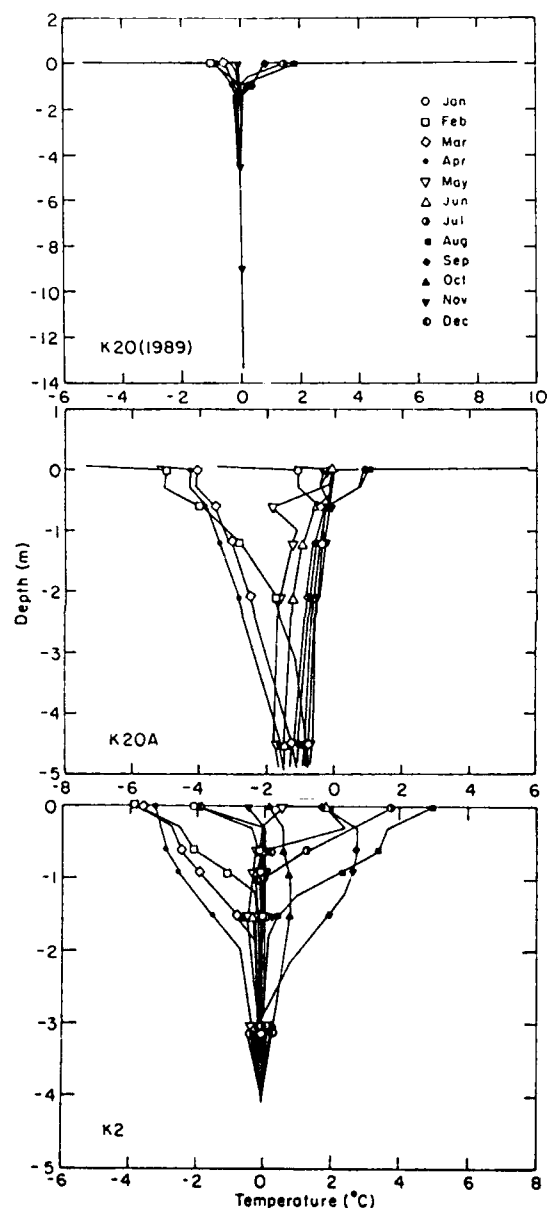

Figure 11. Downhole temperatures for 1989. Seasonal variations are attenuated in K20, exhibiting uniform, relatively stable temperatures, with the unfrozen horizon occurring at about 8.0 to 13.5 m. K20A and K2 show more typical seasonal responses within about 5 m of the surface.

13

Table 1. Ground temperature data from thermistor strings installed in boreholes K20, K20A and K2.

	Depth m	Jan	Feb	Mar	Apr	May	Jun	Jul	Aug	Sep	Oct	Nov	Dec	Annual average
							a. K20 1987							
1	0.05	-1.34	-1.92	-2.48	-1.48	0.12	3.69	5.67	3.83	3.19	-3.20	-4.69	-4.02	-0.22
2	0.0	-0.95	-1.38	-2.03	-1.33	-0.04	0.44	—	—	0.07	-0.22	-0.72	-0.87	—
3	-0.3	-0.23	-0.55	-1.33	-1.11	-0.28	-0.15	0.38	1.41	0.43	-0.02	-0.03	-0.05	-0.13
4	-0.6	-0.05	-0.06	-0.66	-0.88	-0.41	-0.24	-0.16	0.10	0.17	-0.02	-0.02	-0.03	-0.19
5	-0.9	-0.04	-0.05	-0.24	-0.62	-0.40	-0.25	-0.19	-0.14	-0.05	-0.06	-0.06	-0.07	-0.18
6	-1.2	-0.08	-0.08	-0.16	-0.48	-0.38	-0.26	-0.21	-0.19	-0.14	-0.12	-0.11	-0.10	-0.19
7	-1.5	-0.05	-0.06	-0.10	-0.32	-0.30	-0.22	-0.18	-0.16	-0.14	-0.12	-0.10	-0.09	-0.15
8	-2.1	-0.05	-0.05	-0.06	-0.14	-0.17	-0.15	-0.14	-0.13	-0.12	-0.11	-0.10	-0.09	-0.11
9	-3.0	0.12	0.11	0.19	0.19	0.16	0.06	-0.03	-0.07	0.66	0.51	0.35	0.22	0.21
10	-4.5	0.01	0.01	0.00	-0.01	-0.01	-0.02	-0.03	-0.03	-0.02	-0.02	-0.01	-0.01	-0.01
11	-6.0	0.02	0.01	0.00	0.00	-0.01	-0.01	-0.02	-0.02	-0.01	-0.01	-0.01	0.00	-0.01
12	-9.0	0.03	0.06	0.05	0.05	0.04	0.04	0.03	0.03	0.03	0.03	0.04	0.04	0.04
13	-12.0	0.10	0.10	0.09	0.08	0.08	0.07	0.07	0.07	0.08	0.07	0.07	0.05	0.08
14	-13.4	0.07	0.07	0.07	0.06	0.06	0.05	0.05	0.06	0.05	0.05	0.06	0.06	0.06
							b. K20A 1987							
1	0.05	-3.01	-4.87	-5.87	-3.81	0.14	5.56	7.46	3.72	0.18	-1.49	-2.21	-3.42	-0.63
2	0.0	-2.45	-3.69	-5.20	-3.84	-0.12	0.07	1.34	0.96	0.02	-0.05	-0.46	-1.80	-1.27
3	-0.3	-2.10	-3.35	-4.77	-3.42	-0.54	-0.26	0.07	1.15	-0.05	-0.06	-0.09	-1.04	-1.29
4	-0.6	-1.52	-2.66	-4.08	-3.46	-1.08	-0.57	-0.37	0.28	0.21	-0.16	-0.17	-0.50	-1.26
5	-0.9	-1.18	-2.24	-3.66	-3.11	-1.48	-0.80	-0.56	-0.46	-0.36	-0.28	-0.27	-0.38	-1.23
6	-1.2	-0.99	-1.96	-3.23	-3.01	-1.77	-0.99	-0.72	-0.60	-0.49	-0.39	-0.37	-0.40	-1.24
7	-1.5	-0.86	-1.72	-2.97	-3.15	-1.94	-1.11	-0.81	-0.68	-0.56	-0.45	-0.42	-0.42	-1.26
8	-2.1	-0.75	-1.42	-2.50	-2.83	-2.12	-1.28	-0.95	-0.80	-0.67	-0.54	-0.51	-0.47	-1.24
9	-3.0	-0.66	-1.11	-1.91	-2.04	-2.14	-1.44	-1.09	-0.93	-0.78	-0.65	-0.60	-0.55	-1.16
10	-4.5	-0.63	-0.76	-1.17	-1.66	-1.77	-1.50	-1.23	-1.08	-0.93	-0.79	-0.74	-0.68	-1.08
11	-4.9	-0.63	-0.74	-1.12	-1.61	-1.73	-1.49	-1.24	-1.10	-0.95	-0.82	-0.76	-0.70	-1.07
							c. K2 1987							
1	0.05	-4.86	-9.51	-8.24	-3.26	0.91	5.96	8.26	5.36	0.74	-1.22	-4.20	-4.15	-1.18
2	0.0	-3.55	-6.49	-7.37	-3.13	-0.15	2.03	3.80	2.83	1.37	-0.14	-0.79	-2.25	-1.15
3	-0.3	-1.65	-3.94	-5.68	-2.94	0.08	-0.17	0.27	1.69	1.42	0.08	-0.05	-0.08	-0.91
4	-0.6	-0.82	-2.98	-4.95	-2.89	-1.00	-0.39	-0.11	0.79	1.24	0.10	-0.04	-0.06	-0.93
5	-0.9	-0.21	-2.05	-4.14	-2.75	-1.11	-0.51	-0.25	0.12	0.95	0.10	-0.04	-0.05	-0.83
6	-1.2	-0.03	-1.07	-3.25	-2.49	-1.11	-0.53	-0.31	-0.11	0.61	0.11	-0.01	-0.03	-0.69
7	-1.5	-0.04	-0.42	-2.25	-2.14	-1.10	-0.57	-0.35	-0.20	0.17	0.06	-0.02	-0.03	-0.57
8	-2.1	-0.02	-0.02	-0.82	-1.47	-0.96	-0.55	-0.36	-0.27	-0.13	-0.05	-0.04	-0.03	-0.39
9	-3.0	-0.02	-0.01	-0.08	-0.62	-0.64	-0.44	-0.31	-0.25	-0.17	-0.10	-0.08	-0.06	-0.23
10	-4.1	0.06	0.06	0.03	-0.05	-0.17	-0.23	-0.20	-0.18	-0.14	-0.10	-0.08	-0.07	-0.09

Table 1 (Cont'd).

d. K20 1988

Depth, m	Jan	Feb	Mar	Apr	May	Jun	Jul	Aug	Sep	Oct	Nov	Dec	Annual average
0.05	-4.05	-4.35	-3.53	-2.23	—	—	—	—	—	—	—	—	—
0.0	-1.04	-1.67	-1.87	-1.74	0.58	—	—	—	2.23	-0.53	-0.65	-0.91	—
-0.3	-0.18	-0.64	-1.04	-0.35	-0.25	-0.07	1.07	2.11	0.84	0.01	-0.05	-0.03	0.03
-0.6	-0.04	-0.07	-0.52	-0.98	-0.38	-0.20	0.01	0.90	0.46	-0.01	-0.06	-0.04	-0.08
-0.9	-0.07	-0.07	-0.22	-0.70	-0.41	-0.19	-0.19	0.13	0.09	-0.04	-0.07	-0.05	-0.16
-1.2	-0.10	-0.10	-0.19	-0.55	-0.42	-0.26	-0.25	-0.18	-0.13	-0.11	-0.12	-0.11	-0.21
-1.5	-0.09	-0.10	-0.14	-0.38	-0.36	-0.23	-0.23	-0.19	-0.16	-0.13	-0.12	-0.12	-0.19
-2.1	-0.09	-0.09	-0.11	-0.21	-0.25	-0.13	-0.16	-0.10	-0.11	-0.12	-0.12	-0.12	-0.13
-3.0	0.19	0.22	0.27	0.23	0.20	0.25	0.15	0.11	0.06	0.04	0.02	0.03	0.15
-4.5	-0.02	-0.02	-0.03	-0.04	-0.05	-0.04	-0.06	-0.06	-0.05	-0.04	-0.05	-0.05	-0.04
-6.0	-0.01	-0.01	-0.02	-0.03	-0.03	-0.03	-0.04	-0.04	-0.04	-0.03	-0.04	-0.03	-0.03
-9.0	0.03	0.03	0.02	0.02	0.02	0.08	0.02	0.02	0.02	0.02	0.00	0.01	0.02
-12.0	0.07	0.07	0.06	0.05	0.06	0.09	0.05	0.05	0.08	0.05	0.04	0.05	0.06
-13.0	0.06	0.05	0.04	0.04	0.04	0.10	0.05	0.07	0.06	0.05	0.03	0.03	0.05

e. K20A 1988

Depth, m	Jan	Feb	Mar	Apr	May	Jun	Jul	Aug	Sep	Oct	Nov	Dec	Annual average
0.05	-4.689	-5.628	-5.244	-4.597	1.6178	6.4299	7.2476	5.074	—	-2.122	-4.793	-2.926	-0.88
0.0	-3.183	-4.526	-4.612	-4.492	-0.404	0.3549	1.542	1.3253	0.2032	-0.077	-0.237	-0.648	-1.23
-0.3	-2.629	-4.077	-4.32	-4.415	-0.776	-0.187	0.1758	0.2835	0.1074	-0.098	-0.286	-0.651	-1.41
-0.6	-1.914	-3.347	-3.824	-4.091	-0.989	-0.535	-0.356	-0.230	-0.173	-0.164	-0.167	-0.189	-1.33
-0.9	-1.514	-2.867	-3.278	-3.84	-1.621	-0.769	-0.567	-0.452	-0.346	-0.295	-0.273	-0.264	-1.34
-1.2	-1.265	-2.525	-3.227	-3.643	-1.889	-0.966	-0.736	-0.564	-0.474	-0.413	-0.378	-0.354	-1.37
-1.5	-1.076	-2.218	-2.969	-3.419	-2.039	-1.086	-0.834	-0.647	-0.543	-0.472	-0.434	-0.394	-1.34
-2.1	-0.881	-1.806	-2.577	-3.061	-2.199	-1.263	-0.984	-0.773	-0.652	-0.567	-0.521	-0.473	-1.31
-3.0	-0.739	-1.365	-2.071	-2.549	-2.212	-1.425	-1.134	-0.905	-0.773	-0.673	-0.617	-0.555	-1.25
-4.5	-0.670	-0.868	-1.344	-1.666	-1.834	-1.511	-1.288	-1.078	-1.941	-0.833	-0.733	-0.684	-1.12
-4.9	-0.681	-0.854	-1.235	-1.611	-1.802	-1.522	-1.311	-0.814	-0.970	-0.864	-0.799	-0.715	-1.10

f. K2 1988

Depth, m	Jan	Feb	Mar	Apr	May	Jun	Jul	Aug	Sep	Oct	Nov	Dec	Annual average
0.05	-4.63	-6.06	-5.85	-3.85	2.05	7.80	10.00*	9.72	4.75	-1.52	-3.01	-3.46	0.49
0.0	-2.61	-4.38	-4.60	-3.51	0.21	4.16	7.24*	8.47	5.00	0.01	-1.72	-2.39	0.49
-0.3	-0.37	-1.86	-3.14	-3.22	-0.55	2.18	5.56*	7.28	5.15	0.96	-0.02	-0.16	0.98
-0.6	-0.10	-1.16	-2.72	-3.03	-0.68	1.25	4.55*	6.30	5.45	0.71	0.00	-0.11	0.87
-0.9	-0.07	-0.32	-1.99	-2.65	-0.85	-0.01	2.82*	5.49	5.09	1.18	0.04	-0.09	0.72
-1.2	-0.04	-0.06	-1.20	-2.20	-0.88	-0.26	1.62*	4.53	4.91	1.32	0.08	-0.06	0.65
-1.5	-0.04	-0.05	-0.55	-1.66	-0.88	-0.27	0.63*	3.63	4.56	1.37	0.11	-0.05	0.57
-2.1	-0.03	-0.04	-0.09	-0.84	-0.79	-0.15	0.00*	2.46	3.84	1.34	0.09	-0.04	0.48
-3.0	-0.05	-0.05	-0.07	-0.25	-0.56	-0.04	0.10*	1.51	2.89	0.98	-0.01	-0.05	0.37
-4.1	-0.06	-0.06	-0.06	-0.07	-0.22	—	—	—	—	—	-0.08	-0.07	—

*Cable disturbed by black bear. Temperature data from July through Nov. reflect disturbance.

Table 1 (Cont'd). Ground temperature data from thermistor strings installed in boreholes K20, K20A, and K2.

g. K20 1989

	Depth m	Jan	Feb	Mar	Apr	May	Jun	Jul	Aug	Sep	Oct	Nov	Dec	Annual average
1	0.05	-3.33	-5.82	-3.97	-2.53	7.86	9.28	9.45	7.32	0.01	-0.40	-0.52	-0.76	1.38
2	0.0	-0.73	-2.44	-1.48	-1.36	0.74	1.77	3.92	3.65	0.49	-0.10	-0.16	-0.17	0.35
3	-0.3	-0.07	-0.95	-0.70	-0.86	-0.15	-0.12	1.42	1.79	0.79	-0.05	-0.05	-0.07	0.08
4	-0.6	-0.07	-0.05	-0.36	-0.56	-0.20	-0.20	-0.19	0.68	0.57	-0.07	-0.05	-0.04	-0.01
5	-0.9	-0.08	-0.07	-0.12	-0.31	-0.17	-0.15	0.05	0.17	0.26	-0.06	-0.06	-0.05	-0.05
6	-1.2	-0.13	-0.11	-0.17	-0.29	-0.28	-0.25	-0.21	-0.13	0.08	-0.11	-0.12	-0.09	-0.15
7	-1.5	-0.13	-0.12	-0.16	-0.24	-0.25	-0.23	-0.20	-0.18	-0.16	-0.15	-0.13	-0.10	-0.17
8	-2.1	-0.12	-0.11	-0.14	-0.18	-0.09	-0.06	0.08	0.00	0.14	-0.14	-0.12	-0.09	-0.07
9	-3.0	0.02	0.02	0.08	0.09	-0.04	-0.13	-0.13	-0.13	-0.04	-0.11	-0.10	-0.06	-0.04
10	-4.5	-0.06	-0.05	-0.06	-0.06	-0.07	-0.07	-0.07	-0.08	-0.07	-0.02	-0.08	-0.05	-0.06
11	-6.0	-0.05	-0.03	-0.04	-0.04	-0.04	-0.04	-0.05	-0.05	-0.05	-0.05	-0.06	-0.03	-0.04
12	-9.0	0.00	0.00	0.00	0.00	0.02	0.04	0.00	0.00	0.00	0.00	-0.01	-0.06	0.00
13	-12.0	0.03	0.04	0.03	0.03	0.10	0.05	0.07	0.07	0.06	0.07	0.02	0.05	0.05
14	-13.4	0.02	0.04	0.02	0.02	0.08	0.11	0.16	0.12	0.05	0.04	0.02	0.05	0.06

h. K20A 1989

	Depth m	Jan	Feb	Mar	Apr	May	Jun	Jul	Aug	Sep	Oct	Nov	Dec	Annual average
1	0.05	-3.57	-7.42	-5.43	-4.95	—	4.52	5.79	4.41	0.00	-0.96	-2.11	-1.01	-0.97
2	0.0	-1.12	-5.00	-4.12	-4.26	-0.14	-0.07	0.88	0.96	-0.01	-0.06	-0.24	-1.39	-1.13
3	-0.3	-1.10	-5.07	-4.13	-4.30	-0.19	0.06	0.75	0.72	-0.07	-0.12	-0.47	-1.46	-1.20
4	-0.6	-0.41	-3.99	-3.57	-3.84	-1.89	-0.57	-0.29	-0.23	0.18	-0.18	-0.15	-0.16	-1.29
5	-0.9	-0.36	-3.35	-3.30	-3.59	-1.05	-0.79	-0.48	-0.41	-0.33	-0.30	-0.26	-0.24	-1.21
6	-1.2	-0.41	-2.85	-3.10	-5.41	-1.28	-0.97	-0.64	-0.55	-0.46	-0.41	-0.36	-0.34	-1.23
7	-1.5	-0.45	-2.38	-2.89	-3.19	-1.42	-1.09	-0.73	-0.63	-0.53	-0.48	-0.41	-0.38	-1.22
8	-2.1	-0.53	-1.77	-2.57	-2.86	-1.63	-1.26	-0.86	-0.76	-0.63	-0.57	-0.50	-0.46	-1.20
9	-3.0	-0.60	-1.19	-2.11	-2.41	-1.77	-1.41	-0.99	-0.89	-0.75	-0.67	-0.59	-0.54	-1.16
10	-4.5	-0.70	-0.76	-1.35	-1.63	-1.70	-1.49	-1.16	-1.05	-0.92	-0.84	-0.74	-0.69	-1.09
11	-4.9	-0.73	-0.76	-1.31	-1.58	-1.70	-1.51	-1.19	-1.09	-0.95	-0.87	-0.77	-0.72	-1.10

i. K2 1989

	Depth m	Jan	Feb	Mar	Apr	May	Jun	Jul	Aug	Sep	Oct	Nov	Dec	Annual average
1	0.05	-2.99	-4.441	-3.89	-3.361	7.90	6.67	7.25	7.36	0.74	-0.70	-1.13	-3.82	0.80
2	0.0	-2.10	-3.886	-3.69	-3.294	0.52	1.80	3.70	4.93	1.74	0.07	-0.57	-2.15	-0.24
3	-0.3	-0.42	-2.53	-2.77	-3.065	-0.27	2.36	1.41	3.57	2.73	0.53	-0.02	-0.08	0.12
4	-0.6	-0.19	-2.154	-2.55	-2.949	-0.32	-0.22	1.21	3.33	2.69	0.54	-0.03	-0.10	-0.06
5	-0.9	-0.11	-1.154	-1.98	-2.548	-0.48	-0.29	-0.02	2.26	2.58	0.70	0.02	-0.06	-0.09
6	-1.2	-0.09	-0.236	-1.47	-2.122	-0.52	-0.30	-0.14	0.99	2.36	0.76	0.06	-0.04	-0.06
7	-1.5	-0.08	-0.074	-0.84	-1.522	-0.53	-0.33	-0.23	0.37	1.86	0.75	0.09	-0.02	-0.05
8	-2.1	-0.07	-0.053	-0.06	-0.56	-0.49	-0.18	-0.25	-0.18	0.83	0.62	0.12	0.01	-0.02
9	-3.0	-0.07	-0.064	-0.06	-0.074	-0.34	-0.20	-0.22	-0.19	-0.11	0.25	0.07	0.00	-0.08
10	-4.1	-0.08	-0.072	-0.06	-0.066	-0.12	0.09	-0.16	-0.15	-0.12	-0.09	-0.06	-0.06	-0.09

are highly attenuated within 3.0 m of the surface (Fig. 11). Below this depth, ground temperatures do not show a seasonal response. Values increase to slightly above 0°C with little systematic variation from month to month. Thermistor measurements at the 9.0-, 12.0- and 13.4-m depths indicate an average annual value of 0.05°C, significantly higher than anticipated from the estimated MAAT and MAGT values for this location. Temperatures at this depth clearly do not simply reflect the effects of local climatic conditions on the regional geothermal heat flux.

Temperatures within permafrost can normally be defined using steady state, one-dimensional heat conduction theory. According to the Fourier heat conduction law (e.g., Gold and Lachenbuch 1973)

$$q = K_n G_n \qquad (4)$$

where G_n is the thermal gradient of layer n, K_n is the thermal conductivity of layer n, and q is the rate of heat conducted per unit area. The thermal gradient is simply defined as

$$G_n = \frac{dt}{dz} \qquad (5)$$

where t is temperature and z is depth.

Locally, the value of q can be assumed to be identical in each borehole. Because subsurface materials at K20 and K20A are basically identical (although the thickness of the colluvium is less at K20A), the thermal conductivity of the stratigraphic sequence can be assumed to be similar as well. Therefore, we also assume that the temperature gradient and range in subsurface temperatures at K20 should be the same overall as in K20A unless modified by other external factors.

Comparison of the K20A and K20 data shows no similarity to the temperatures to the 5-m depth nor projected temperatures for K20A from the 5-m depth to the equivalent 13-m depth of K20. Projected ground surface temperatures are also dissimilar. A mean annual surface temperature projected from the borehole data of K20 would be much higher than expected, ranging from –0.15 to –0.2°C for 1987 to 1989. These data also indicate a modified heat flux at depth.

The relatively constant temperatures and their limited range suggest that heat conducted by groundwater is locally disturbing the thermal regime in K20 and maintaining temperatures above the freezing point. In the 3 years of record, the uniform temperatures slightly increased (0.04 to 0.14°C range) in the summer months of May through September of 1988 and 1989, particularly in the months of June and July, in the unfrozen zone (Table 1). Ground temperatures above this zone do not show a corresponding increase, and, in particular

from about the 3.5-m depth to the 9.0-m depth, show little variation. In addition the temperature increases take place too rapidly to be a response to seasonal surface warming. In the remaining months of 1988 and 1989, as well as all of 1987, there were virtually no variations in ground temperatures (≤0.03°C) below 3 m depth. Records from the nearest climatic station at Fairbanks indicate that May through September are typically the wettest and warmest months in this region (NOAA 1989). Both 1988 and 1989 had comparable average air temperatures during the summer months, but normal or above average precipitation in May and, in particular, June when 2.26 and 2.53 in. (57.4 and 64.3 mm) of precipitation, respectively, fell (0.87 and 1.14 in. [22.1 and 28.0 mm] above normal). During 1987, air temperatures were comparable, but precipitation was below normal each month, with only 1.02 in. (25.9 mm) in June and 6.43 in. (163.3 mm) for the year, about 5 in. (127 mm) below normal.

Thus, there is an apparent relationship between the amount of precipitation and the slight increase in ground temperatures during summer, suggesting that the increase may have resulted from infiltration or recharge of the groundwater in the fracture during May and June. Relatively constant or slightly decreasing temperatures would be expected during the winter season when seasonally frozen ground and low air temperatures would severely restrict or eliminate groundwater recharge. If groundwater recharge was low prior to freezeup, a progressive drop in groundwater discharge in the winter months could result in a reduction in heat flux and a decrease in the temperature in the outer fringe of the thawed zone in the fall and winter. Thus, although the range in variations in the ground temperatures fall within the accuracy of the thermistors, the consistent increase in the absolute temperatures and apparent association with summer precipitation lend support to the idea of a groundwater source for the continuously unfrozen conditions.

To provide some verification of the near 0°C temperature measurements, samples of the water–sediment mixture from borehole K20 and of leachate extracted from the same sample were analyzed to determine whether its freezing point was 0°C or depressed by the presence of salts to a more negative value. This procedure was considered important in lieu of the accuracy of the temperature measurements to determine if the water could be at subfreezing temperatures and thus static within the permafrost.

A sample from the water–sediment mixture was placed in a controlled temperature cell and gradually cooled at 0.01°C increments. Unfrozen water content was monitored using the NMR technique (Tice et al. 1978). It began freezing at 0°C with pore ice formation initiated.
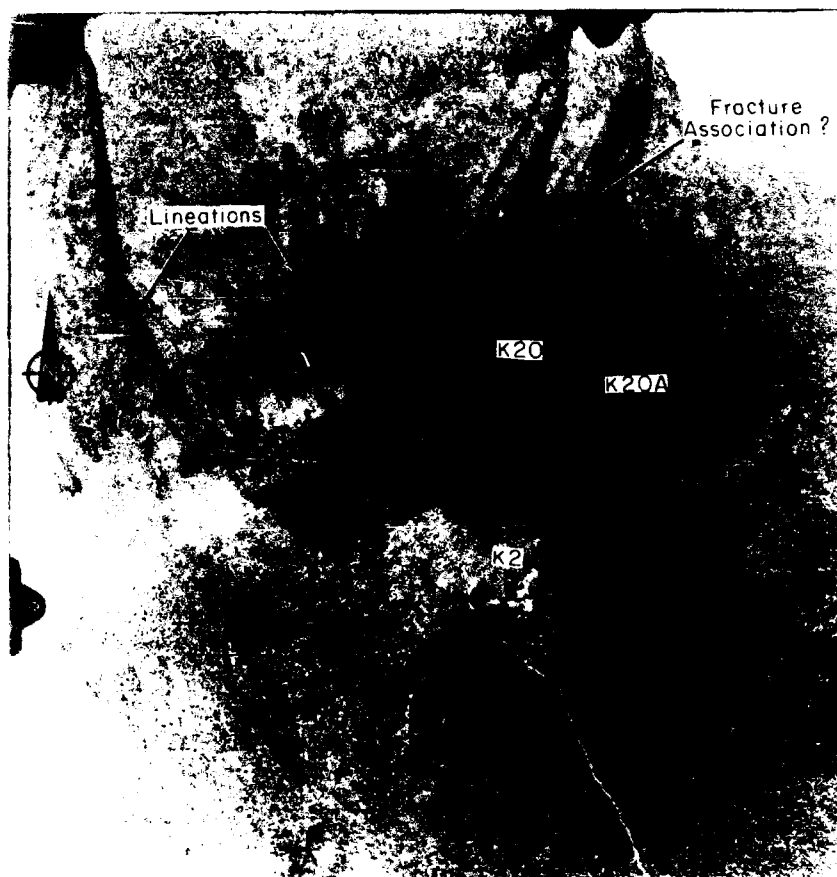
Figure 12. Aerial photograph of the Caribou Peak area on 12 July 1977, showing the approximately parallel linear arrangement to the vegetation. The darker lineations result from an increased cover composed of alder, willow and taller black spruce. The fractures identified by radar profiling (dashed lines) appear to intersect the interface between the weathered rock and the colluvium.

A leachate sample was also analyzed by ion chromatography to examine the presence of principal salt-forming cations. This analysis indicated quantities estimated at less than several parts per million, with the probability that there was virtually no freezing point depression.

These analyses support the credibility of the positive, near 0°C temperature measurements, and that the groundwater must be continuously replenished from a fresh water source.

Thus, the generally stable and positive near 0°C temperatures within the fracture zone, the highly attenuated seasonal temperature variations, the apparent lack of correlation in ground temperatures to local climatic conditions, and the steep temperature gradient are evidence of a thermal disturbance caused by heat conducted by groundwater flowing within the fractures throughout the year.

Vegetation patterns and fracture locations

Changes in the vegetation covering the northern slope of Caribou Peak form a mostly linear pattern (Fig. 12). Vegetative lineations, which trend generally north–south and lie approximately parallel to one another, reflect shifts in the composition and percentage of cover. While the majority of the northern face is covered by an open black spruce forest with scattered alder, the vegetation in the lineations is a denser cover of taller black spruce, alder and willow. These differences in the vegetation indicate slightly warmer and wetter conditions here than in the areas immediately adjacent to them.

In addition, the vegetative pattern can be differentiated into those lineations that are discontinuous and generally disappear within the upper two-thirds of the slope and those that are continuous downslope and located within gullies incised into the bedrock of about

18

the lower one-third of the northern face (Fig. 12). These gullies commonly converge, forming seasonal tributaries to Poker Creek. Within the upper two-thirds of the slope, neither of these groups of lineations are associated with such changes in surface relief.

The cause of the vegetative pattern appears to be related to the fractures within the bedrock. A plot of the approximate positions of radar profiles on an aerial photograph (Fig. 12) suggests that the water-bearing fractures intersect the interface between the bedrock and colluvial overburden beneath or adjacent to the vegetative lineations (Fig. 13). Thus, the thicker vegetation apparently occurs where higher ground temperatures and increased availability of moisture result from groundwater discharge through the fractures.

The association of the continuous lineations with the intersecting gullies suggests that a seasonal drainage (there are no perennial streams here) results from seasonal increases in groundwater discharge from the fractures, coupled with surface runoff from snowmelt or major rainfall events, or both. Deeper weathering of bedrock in the fracture zones may be in part responsible for gully development within the lower slope, as well as for concentrating seasonal surface runoff in the upper reaches of these lineations. The discontinuous lineations imply enhanced temperatures and moisture conditions attributable to the presence of fractures or joints, but limited surface runoff or an absence of groundwater flow. The occurrence of other continuous vegetative lineations elsewhere on this northern slope of Caribou Peak as well as others in the watershed implies that additional water-bearing fractures and localized thaw zones may exist in this region.

Groundwater origin

The source of water flowing within the fractures is somewhat problematic, but limited by the local geology and site geography. Both the trend of the fractures defined by the radar profiles and their apparent associa-

tion with the vegetative patterns across the slope indicate that there must be a source at depth in the upper elevations of Caribou Peak. Yet the borehole location is only 60 m in elevation below the Peak's crest. The fact that multiple fractures exist, each exhibiting reflectors corresponding to water flow, indicates that the source is probably not a single spring outcropping near the crest, but rather a more pervasive aquifer. It should be noted that no springs have been observed within this area. The ground temperatures also require that water moving through the fractures be sufficiently warm to maintain a localized unfrozen condition within the otherwise permanently frozen bedrock that encompasses them. In addition, the chemical and NMR analyses indicate the source must be fresh water.

Our hypothesis concerning the origin of the groundwater is based upon these observations and the geologic limitations of this site. The general north–south strike and low angle, easterly dip of the fractures indicate that they bisect the hill and probably continue through Caribou Peak to its southern and southeastern slopes (Fig. 14). Vegetative patterns and associated rock outcrops identified on aerial photographs also appear continuous from the north to south face. If they are continuous through the hill, the fractures must intersect the non-permafrost zone below the south face. An aquifer within the unfrozen bedrock here could provide a source of water for the fractures.

Borehole temperature measurements at mid-slope on the southern face confirm that permafrost is absent. Mean annual surface temperatures range from 0.4 to 2.2°C, and ground temperatures at 10 m depth range from 0.9 to 1.9°C (Collins et al. 1988). Since groundwater temperatures approximate the mean annual air temperatures, we anticipate that groundwater within this non-permafrost area would have a temperature somewhere within the range of 0.9 to 1.9°C. This range would be consistent with groundwater temperatures in the Fairbanks region of an average 1.7°C as reported by Williams (1970).
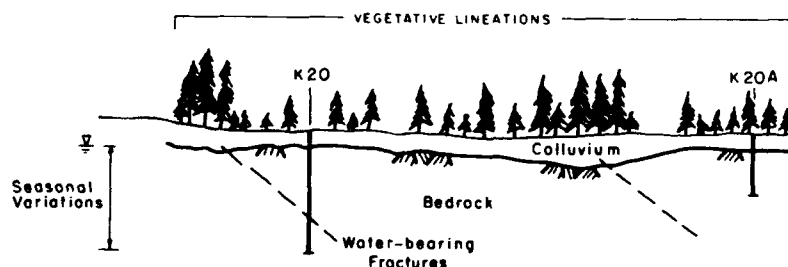

Figure 13. Idealized diagram showing a possible relationship between water-bearing fractures and vegetative lineations.

Thus, if we assume that the fractures intersect an aquifer, water may be transmitted within them and along their entire length from the warmer southern side to the northern face (Fig. 14). Discharge along the length of the fracture's intersection with the colluvium would be consistent with the continuous nature of the vegetative lineations. Water can move within the fractures, however, only if the combination of permafrost thickness, permafrost temperatures, groundwater temperatures and flow zone properties result in sufficient flow rates and heat flux to maintain an unfrozen zone continuously. The water's temperature must remain above freezing while it is flowing through the frozen rock.

The air and ground temperature measurements suggest that the perennially frozen bedrock probably does not exceed $-1.3°C$ in temperature at its coldest point near the 10-m depth. The thickness of permafrost on the north face is unknown, but it probably is not very thick, as is characteristic of this region (Ferrians et al. 1969, Williams 1970). An approximate depth to the base of permanently frozen ground can be determined from the ground temperatures in boreholes K20A and K2, if we assume that q and K (eq 4 and 5) are constant at this location. Calculated mean annual temperature gradients yield an estimated depth to the base of permafrost (0°C depth) of 10 m at K2 and 40 m at K20A. These relatively shallow depths indicate a thinning of perennially frozen ground to the crest of Caribou Peak, as expected.

If groundwater is moving within the fractures from the southern to northern side, we can assume that its initial temperature would be approximately 1.5°C and that it must flow through the estimated 35 m of frozen materials in the K20 borehole area, cooling to slightly above 0°C. The frozen ground temperatures would gradually decrease from 0°C at about 40 m depth below the surface to about $-1.3°C$ at 10 m depth beneath it. The unfrozen zone or talik adjacent to the fracture would extend outward and parallel to the fracture a short distance, dependent upon the groundwater heat flux (Fig. 14).

Once a flow system is established, a thermal equilibrium would necessarily develop, offset only by seasonal warmings from groundwater recharge by major precipitation events during summer. Such seasonal warmings were suggested by the slight increases in borehole K20 ground temperatures from May to August. Heat conducted by the water from the southern, non-permafrost zone must maintain the unfrozen condition, or the zone would refreeze, with ice formation terminating groundwater movement. Once such a system is established and stabilized, heat conducted by the groundwater could maintain the unfrozen state (e.g.,

Williams 1970). If, however, groundwater discharge through the zone decreases, temperatures at the outer fringe of the zone would begin to decrease and initiate freezing-in of the fracture talik.

Rigorous calculations to determine if this is theoretically possible at this site would require data not available to us, principally the actual location of the aquifer relative to fracture discharge, the relative "permeability" of the fracture that controls the rate of flow, and the hydraulic head. Movement within fractures can be relatively rapid, far exceeding that which would depend upon the permeability of the bedrock itself. Groundwater movement from subpermafrost aquifers through a permafrost horizon in bedrock fractures has been described at various locations by Hopkins et al. (1955), Williams and Van Everdingen (1973), Tolstikhin and Tolstikhin (1974) and Ivanik and Veselovskiy (1976), among others. Physical reasoning suggests that flow could occur at a rate sufficient to maintain these near 0°C water temperatures, inhibit freezing and maintain the locally thawed zone through this relatively thin, warm permafrost in a manner analogous to water movement through fractures in temperate glacier ice.

CONCLUSION

The radar survey has identified a fracture in the quartz–muscovite schist bedrock with groundwater flowing in it as the source of the anomalous unfrozen zone within borehole K20. The surveys indicate that several fractures with groundwater flow exist in the surveyed area of the slope, but were not intersected by other drill holes. The uniformity of the near 0°C ground temperatures measured over the last 3 years indicates both the permanence of the unfrozen zone and a requirement for the flow of water through the fracture. The distribution of the water-bearing fractures in relation to the vegetative pattern of the north-facing slope suggests that they act as both water sources and water transmitters from the peak to the valley bottom, enhancing the growth of vegetation where they outcrop below the colluvial cover. The ultimate source of the groundwater, which constantly remains above freezing and thus remains an active flow system annually, is unknown, but may include an aquifer within the hill that penetrates the permafrost beneath the northern slope along permeable, hydraulic anisotropies created by the bedrock fractures that intersect the unfrozen south-facing slope (Fig. 14). Future work to verify the source of water in the fractures should include detailed field studies of the groundwater system through radar surveying of the fracture distribution in Caribou Peak, and drilling and analysis of the groundwater flow pattern and temperatures.

20
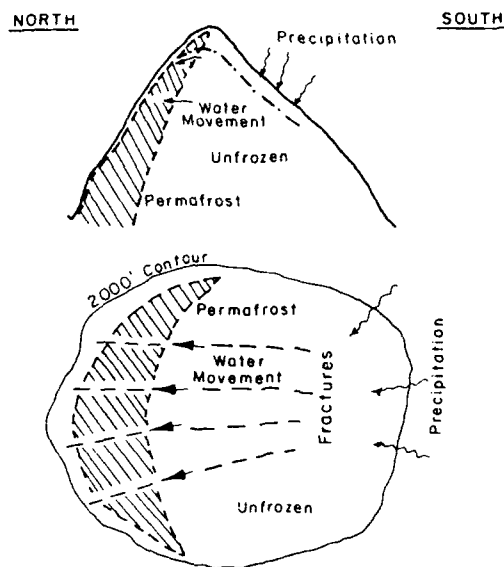
a. Cross section of Caribou Peak, view to east (top) and map view of horizontal slice through Caribou Peak.
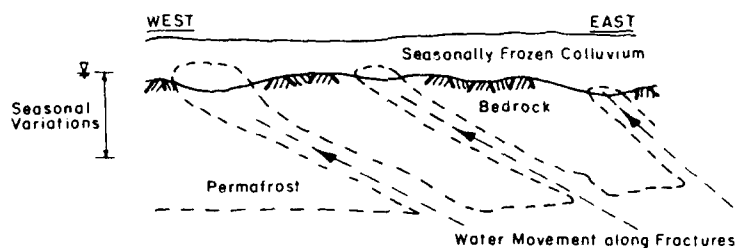
b. Cross section parallel to transect 1, view to north.

Figure 14. Schematic model of the apparent relationship between fractures, groundwater occurrence and vegetation. The hypothesized source of groundwater is an aquifer beneath the non-permafrost southern slope that is intersected by the fractures, which then transmit this water through the permafrost horizon of the northern face.

The presence of unfrozen zones of this type requires consideration when predicting the distribution of permafrost in the Interior region. Similar patterns to the vegetation on other north-facing slopes suggest that thawed zones and groundwater systems associated with bedrock fractures may occur elsewhere within the watershed region.

Groundwater flow on this northern slope discharges into Poker Creek. This discharge contributes to the baseflow of the watershed, but has not previously been considered. It may be important to understanding higher than normal winter flows and baseflow recession in watersheds underlain by discontinuous permafrost (e.g.,

Dingman 1971, Haugen et al. 1982), as well as the source of water forming extensive aufeis within the Poker Creek valley bottom each winter.

Finally, this study has verified the ability of impulse radar operating at high frequency to identify localized unfrozen zones associated with groundwater flow in perennially frozen bedrock.

LITERATURE CITED

Annan, A.P. and J.L. Davis (1976) Impulse radar sounding in permafrost. *Radio Science,* 11(4): 383–394.

21

Arcone, S.A. and A.J. Delaney (1987) Airborne river-ice thickness profiling with helicopter-borne UHF short pulse radar. *Journal of Glaciology*, **33**(115): 330–340.

Arcone, S.A., and A.J. Delaney (1989) Investigations of dielectric properties of some frozen materials using cross-borehole radiowave pulse transmissions. USA Cold Regions Research and Engineering Laboratory, CRREL Report 89-4.

Arcone, S.A., A.J. Delaney and D.J. Calkins (1989) Water detection in the coastal plains of the Arctic National Wildlife Refuge using helicopter-borne short pulse radar. USA Cold Regions Research and Engineering Laboratory, CRREL Report 89-7.

Boucher, R. and L. Galinovsky (1989) Radan 3.0 signal processing software. North Salem, New Hampshire: Geophysical Survey Systems, Inc.

Brown, R.J.E. and T.L. Péwé (1973) Distribution of permafrost in North America and its relationship to the environment: A review, 1963–1973. In *Proceedings of Permafrost: North American Contribution to Second International Conference*. Washington, D.C.: National Academy of Sciences, p. 71–100.

Campbell, M.J., and J. Ulrichs (1969) Electrical properties of rocks and their significance for lunar radar observations. *Journal of Geophysical Research*, **74**(25): 5867–5881.

Cederstrom, D.J. (1963) Ground water resources of the Fairbanks area, Alaska. U.S. Geological Survey, Water Supply Paper 1590.

Collins, C. (1986) Installation of long-term ground temperature monitoring sites in the Caribou–Poker Creeks Research Watershed. USA Cold Regions Research and Engineering Laboratory, CRREL Technical Note, May.

Collins, C.M., R.K. Haugen and R.A. Krieg (1988) Natural ground temperatures in upland bedrock terrain, Interior Alaska. In *Proceedings, Permafrost, Fifth International Conference*, vol.1. Trondheim, Norway: Tapir Pubs., p. 56–60.

Cumming, W. A. (1952) The dielectric properties of ice and snow at 3.2 centimeters. *Journal of Applied Physics*, **23**(7): 768–773.

Delaney, A.J. and S.A. Arcone (1984) Dielectric measurements of frozen silt using time domain reflectometry. *Cold Regions Science and Technology*, **9**: 39–46.

Delaney, A.J., S.A. Arcone and E.F. Chacho (1990) Winter short-pulse radar studies on the Tanana River, Alaska. *Arctic*, **43**(3): 244–250.

Dingman, S.L. (1971) Hydrology of the Glenn Creek Watershed, Tanana River basin, central Alaska. USA Cold Regions Research and Engineering Laboratory, CRREL Research Report 297.

Engheta, N., C.H. Pappa and C. Elachi (1982) Ra-diation patterns of interfacial dipole antennas. *Radio Science*, **17**(6): 1557–1566.

Ferrians, O.J., Jr., R. Kachadoorian and G.W. Greene (1969) Permafrost and related engineering problems in Alaska. U.S. Geological Survey, Professional Paper 678.

Forbes, R.B. and F.R. Weber (1982) Bedrock geologic map of the Fairbanks Mining District, Alaska. Fairbanks, Alaska: Alaska Division of Geological and Geophysical Surveys, Open-File Report 170.

Gold, L.W. and A.H. Lachenbruch (1973) Thermal conditions in permafrost—a review of North American literature. In *Proceedings, Permafrost, Second International Conference*. Washington, D.C.: National Academy of Sciences, p. 3–26.

Haugen, R.K., C.W. Slaughter, K.E. Howe and S.L. Dingman (1982) Hydrology and climatology of the Caribou–Poker Creeks Research Watershed, Alaska. USA Cold Regions Research and Engineering Laboratory, CRREL Report 82-26.

Haugen, R.K., S.I. Outcalt and J.C. Harle (1983) Relationships between estimated mean annual air and permafrost temperatures in north-central Alaska. In *Proceedings, Permafrost, Fourth International Conference, July 1983*. Washington, D.C.: National Academy of Sciences Press, p. 462–467.

Hoekstra, P., P.V. Sellmann and A.J. Delaney (1975) Ground and airborne resistivity surveys of permafrost near Fairbanks, Alaska. *Geophysics*, **40**(4): 641–656.

Hopkins, D.M., T.N.V. Karlstrom, et al. (1955) Permafrost and ground water in Alaska. U.S. Geological Survey, Professional Paper 264-F.

Ivanik, V.M. and N.V. Veselovskiy (1976) Role of ground waters in the formation of the chemistry of river waters during the summer–autumn low-flow period in permafrost regions. *Soviet Hydrology: Selected Papers*, **15**(3): 226–234.

Lunardini, V.J. (1981) *Heat Transfer in Cold Regions*. New York: Van Nostrand Reinhold Company.

NOAA (1989) Local climatological data: Annual summary with comparative data, Fairbanks, Alaska. Asheville, North Carolina: National Oceanic and Atmospheric Administration, National Climatic Data Center.

Péwé, T.L. and J.W. Bell (1975) Miscellaneous field studies map, Fairbanks D-2 Quadrangle. U.S. Geological Survey, Map MF-669B.

Rieger, S., C.E. Furbush D.B. Schoephorster, H. Sommerfield and L.C. Geiger (1972) Soils of the Poker–Caribou Creeks Research Watershed. USA Cold Regions Research and Engineering Laboratory, Technical Report 236.

Robinson, M.S., T.E. Smith and P.A. Metz (1990) Bedrock geology of the Fairbanks Mining District.

Fairbanks, Alaska: Alaska Division Geological and Geophysical Surveys, Professional Report 106.

Tice, A.R., C.M. Burrous and D.M. Anderson (1978) Determination of unfrozen water in frozen soil by pulsed nuclear magnetic resonance. In *Proceedings of Third International Conference on Permafrost, July 1978, Edmonton, Canada,* p. 149–155.

Tolstikhin, N.I. and O.N. Tolstikhin (1974) Groundwater and surface water in the permafrost region. Translation, 1978, Inland Waters Directorate, Water Resources Branch, Ottawa, Canada. Technical Bulletin No. 97.

Topp, G. C., J.L. Davis and A.P. Annan (1980) Electromagnetic determination of soil water content: measurements in coaxial transmission lines. *Water Resources Research,* **16**(3): 574–582.

Wahrhaftig, C. (1965) Physiographic divisions of Alaska. U.S. Geological Survey, Professional Paper 482.

Williams, J.R. (1970) Ground water in the permafrost regions of Alaska. U.S. Geological Survey, Professional Paper 696.

Williams, J.R. and R.O. Van Everdingen (1973) Ground water investigations in permafrost regions of North America: A review. In *Proceedings, Permafrost, Second International Conference.* Washington, D.C., National Academy of Sciences, p. 435–446.

REPORT DOCUMENTATION PAGE

Public reporting burden for this collection of information is estimated to average 1 hour per response, including the time for reviewing instructions, searching existing data sources, gathering and maintaining the data needed, and completing and reviewing the collection of information. Send comments regarding this burden estimate or any other aspect of this collection of information, including suggestion for reducing this burden, to Washington Headquarters Services, Directorate for Information Operations and Reports, 1215 Jefferson Davis Highway, Suite 1204, Arlington, VA 22202-4302, and to the Office of Management and Budget, Paperwork Reduction Project (0704-0188), Washington, DC 20503.

1. AGENCY USE ONLY (Leave blank)	2. REPORT DATE October 1991	3. REPORT TYPE AND DATES COVERED

4. TITLE AND SUBTITLE Geophysical Investigations of an Anomalous Unfrozen Zone, Caribou Peak, Alaska	5. FUNDING NUMBERS
6. AUTHORS Daniel E. Lawson, Steven A. Arcone and Charles M. Collins	

7. PERFORMING ORGANIZATION NAME(S) AND ADDRESS(ES) U.S. Army Cold Regions Research and Engineering Laboratory 72 Lyme Road Hanover, N.H. 03755-1290	8. PERFORMING ORGANIZATION REPORT NUMBER CRREL Report 91-17

9. SPONSORING/MONITORING AGENCY NAME(S) AND ADDRESS(ES)	10. SPONSORING/MONITORING AGENCY REPORT NUMBER

11. SUPPLEMENTARY NOTES

12a. DISTRIBUTION/AVAILABILITY STATEMENT Approved for public release; distribution is unlimited. Available from NTIS, Springfield, Virginia 22161.	12b. DISTRIBUTION CODE

13. ABSTRACT *(Maximum 200 words)*

The occurrence of unfrozen materials and groundwater flow on a north-facing slope in interior Alaska is important to recognize, both for predicting the spatial distribution of perennially frozen ground as well as for understanding watershed hydrology. An anomalous unfrozen zone or talik was located on the northern slope of Caribou Peak by drilling in April 1985. Impulse radar surveying of the area immediately adjacent to this drill hole, as well as on three transects upslope of its location, revealed that the unfrozen zone is the result of groundwater flow in the bedrock along a relatively planar zone, interpreted as a fracture. This fracture and two others located by the radar are continuous in the direction of the slope, trending generally N20°E and dipping about 9° east. Geologic logs indicate that the drill hole intersected a fracture in the bedrock, a quartz–muscovite schist, at a depth of about 8.5 to 9.0 m. Downhole measurements show ground temperatures at this depth are generally uniform and slightly above freezing throughout the year, suggesting continuous flow of groundwater within the planar structure. Analysis of the freezing point of the groundwater sample indicates normal freezing beginning at 0°C, while ion chromatography indicated that the water was fresh and not highly mineralized. Vegetation patterns, coupled with the borehole location and fracture orientation, suggest that flow originates within the upper and central parts of the peak and discharges into the valley of Poker Creek. The source of the groundwater is unknown, but appears to be an aquifer in the south-facing, non-permafrost side of Caribou Peak that is intersected by the north–south striking fractures. These fractures then transmit the water to the northern face and channel it through the permanently frozen layer beneath this side. In addition to identifying these unfrozen, localized groundwater flows within perennially frozen bedrock, the radar profiles also revealed signatures that suggest a transition in unfrozen water content within the marginally frozen colluvium.

14. SUBJECT TERMS			15. NUMBER OF PAGES 29
Alaska	Impulse radar	Permafrost hydrology	
Groundwater	Permafrost distribution		16. PRICE CODE

17. SECURITY CLASSIFICATION OF REPORT UNCLASSIFIED	18. SECURITY CLASSIFICATION OF THIS PAGE UNCLASSIFIED	19. SECURITY CLASSIFICATION OF ABSTRACT UNCLASSIFIED	20. LIMITATION OF ABSTRACT UL